The rate of change in Ca^{2+} concentration controls sperm chemotaxis

Luis Alvarez,[1] Luru Dai,[2] Benjamin M. Friedrich,[3] Nachiket D. Kashikar,[1] Ingo Gregor,[4] René Pascal,[1] and U. Benjamin Kaupp[1]

[1]Department of Molecular Sensory Systems, Center of Advanced European Studies and Research (caesar), 53175 Bonn, Germany
[2]National Center for Nanoscience and Technology, Beijing 100190, China
[3]Department of Materials and Interfaces, Weizmann Institute of Science, 76100 Rehovot, Israel
[4]Third Institute of Physics, Faculty of Physics, Georg-August University, 37077 Göttingen, Germany

During chemotaxis and phototaxis, sperm, algae, marine zooplankton, and other microswimmers move on helical paths or drifting circles by rhythmically bending cell protrusions called motile cilia or flagella. Sperm of marine invertebrates navigate in a chemoattractant gradient by adjusting the flagellar waveform and, thereby, the swimming path. The waveform is periodically modulated by Ca^{2+} oscillations. How Ca^{2+} signals elicit steering responses and shape the path is unknown. We unveil the signal transfer between the changes in intracellular Ca^{2+} concentration ($[Ca^{2+}]_i$) and path curvature (κ). We show that κ is modulated by the time derivative $d[Ca^{2+}]_i/dt$ rather than the absolute $[Ca^{2+}]_i$. Furthermore, simulation of swimming paths using various Ca^{2+} waveforms reproduces the wealth of swimming paths observed for sperm of marine invertebrates. We propose a cellular mechanism for a chemical differentiator that computes a time derivative. The cytoskeleton of cilia, the axoneme, is highly conserved. Thus, motile ciliated cells in general might use a similar cellular computation to translate changes of $[Ca^{2+}]_i$ into motion.

Introduction

The flagellum of sperm serves both as a propeller and antenna that detects chemical cues released by the egg or associated structures (Kaupp et al., 2003, 2008). The binding of chemoattractant molecules to surface receptors initiates a series of signaling events that produce Ca^{2+} signals in the flagellum (Matsumoto et al., 2003; Wood et al., 2007; Kaupp et al., 2008; Shiba et al., 2008). Chemotactic signaling and behavior are most advanced in sperm of the sea urchin *Arbacia punctulata*. It involves binding of resact, the chemoattractant, to a receptor guanylyl cyclase, a rapid rise of the cellular messenger cyclic guanosine monophosphate (cGMP; Kaupp et al., 2003), a hyperpolarization as a result of the opening of K^+-selective cyclic nucleotide-gated ion channels (Strünker et al., 2006; Galindo et al., 2007; Bönigk et al., 2009), and, finally, the opening of voltage-dependent Ca_v channels. The periodic stimulation of sperm during circular swimming in a chemoattractant gradient entrains periodic Ca^{2+} signals and alternating periods of high path curvature (turn) and low path curvature (run) that result in a looping swimming path toward the egg (Böhmer et al., 2005; Friedrich and Jülicher, 2007; Wood et al., 2007; Guerrero et al., 2010a,b).

The relationship between intracellular Ca^{2+} concentration ($[Ca^{2+}]_i$) and flagellar beat or path curvature has been primarily studied in sperm that had been demembranated by detergents and reactivated by addition of ATP and cAMP (Lindemann and Lesich, 2009). These studies show that the flagellar beat is more asymmetrical at high $[Ca^{2+}]_i$ and more symmetrical at low $[Ca^{2+}]_i$ (Brokaw, 1979; Lindemann and Goltz, 1988; Lindemann et al., 1991). The action of Ca^{2+} on the flagellar beat is mediated by CaM, is relatively slow (on a minute time scale), and is modulated by cAMP (Lindemann et al., 1991). Although these studies highlighted the importance of Ca^{2+} and cAMP in demembranated sperm, for several reasons, the significance for

Correspondence to Luis Alvarez: luis.alvarez@caesar.de; or U. Benjamin Kaupp: u.b.kaupp@caesar.de

N.D. Kashikar's present address is Neurobiology Division, Medical Research Council Laboratory of Molecular Biology, Cambridge CB2 0QH, England, UK.

B.M. Friedrich's present address is Max Planck Institute for the Physics of Complex Systems, 01187 Dresden, Germany.

Abbreviations used in this paper: AM, acetoxymethyl ester; ASW, artificial sea water; cGMP, cyclic guanosine monophosphate.

The Rockefeller University Press $30.00
J. Cell Biol. Vol. 196 No. 5 653–663
www.jcb.org/cgi/doi/10.1083/jcb.201106096

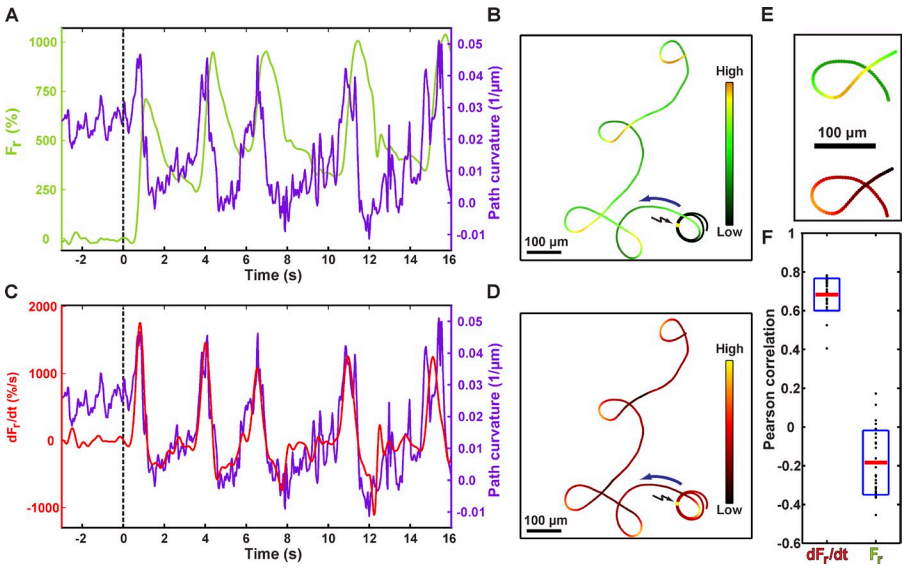

Figure 1. **Time derivative of $[Ca^{2+}]_i$ controls curvature of swimming path.** (A) Changes in $[Ca^{2+}]_i$ and path curvature κ. (B) Color-coded F_r along the swimming path of a cell. The blue arrow indicates the swimming direction. After photorelease of cGMP (black arrow), the cell displays Ca^{2+} oscillations and abandons swimming in closed circles. Of note, $[Ca^{2+}]_i$ was still rising even after the curvature peaked. (C) Time course of the time derivative dF_r/dt and κ superimposes. (A and C) Photolysis of caged cGMP was at t = 0 (dashed lines). (D) Color-coded dF_r/dt along the path of the same cell as in B. (E) Detail of the swimming path. F_r is maximal while the cell swims straight, whereas dF_r/dt is maximal when the cell turns. (F) Pearson correlation between path curvature and dF_r/dt or F_r. Individual data points are displayed as black circles (n = 27), mean correlation is in red, and SD is in blue (box length is twice the SD).

intact motile sperm is limited. First, sperm from both marine invertebrates and mammals respond to stimulation with a rapid Ca^{2+} signal and motor response on the subsecond to second time scale (Kaupp et al., 2003; Böhmer et al., 2005; Wood et al., 2005; Strünker et al., 2006, 2011; Kilic et al., 2009; Guerrero et al., 2010a). However, Ca^{2+} experiments in demembranated sperm lacked time resolution, and, consequently, rapid or transient changes in flagellar beat might have been missed. Second, the Ca^{2+} action critically depends on the extraction and reactivation protocol, giving rise to a wide range of Ca^{2+} sensitivities (Gibbons and Gibbons, 1972; Okuno and Brokaw, 1981). Third, in reactivated flagella, the concentration, dynamics, and location of molecular components important for flagellar bending (Goltz et al., 1988; Salathe, 2007) might have been severely altered. Finally, in intact sperm, high $[Ca^{2+}]_i$ levels persist during low path curvature, i.e., straight swimming (Böhmer et al., 2005; Wood et al., 2005; Shiba et al., 2008; Guerrero et al., 2010a; Kambara et al., 2011), challenging the view that steady-state $[Ca^{2+}]_i$ controls the flagellar beat directly. To overcome these limitations, time-resolved measurements of changes in $[Ca^{2+}]_i$ and motor response in intact swimming sperm are required.

Here, we study Ca^{2+} signals and steering responses of sperm while moving in a gradient of chemoattractant or after the release of the second messenger cGMP via photolysis of caged compounds. We identify the signal transfer function between $[Ca^{2+}]_i$ and path curvature and analyze how the waveform of the Ca^{2+} signal controls the swimming path. Finally, we propose a chemical differentiator model by which cells translate the time derivative of Ca^{2+} signals to modulate the flagellar beat.

Results

Time derivative of $[Ca^{2+}]_i$ controls the path curvature

To understand how changes in $[Ca^{2+}]_i$ control the chemotactic steering response, we studied the dynamic relationship between $[Ca^{2+}]_i$ and path curvature. Using caged compounds, Ca^{2+} oscillations were evoked by a step increase of either cGMP or the chemoattractant resact (Böhmer et al., 2005). First, we stimulated sperm by flash photolysis of caged cGMP and recorded the relative changes in fluorescence (F_r) of the Ca^{2+}-sensitive dye Fluo-4. Binding of Ca^{2+} to and unbinding from BAPTA-derived fluorescent indicators occur within a few milliseconds (Naraghi, 1997; Faas et al., 2011), whereas Ca^{2+} signals occur on a subsecond to second time scale. Therefore, the kinetics of Ca^{2+} signals is not compromised by the kinetics of the dye. In addition, Fluo-4 fluorescence scales linearly with the $[Ca^{2+}]_i$ for the regimen of concentrations found in sperm during chemotaxis (Fig. S1). Unstimulated sperm swam in circles with the net swimming speed v_0 = 120 ± 13 µm/s (mean ± SD; n = 26) and constant path curvature κ_0 = 39 ± 6 mm^{-1}, corresponding to a radius of the swimming circle r_0 = 26 ± 4 µm and a circle period $T = 2\pi/(v_0\kappa_0)$ = 1.4 ± 0.2 s. Photorelease of cGMP elicited a train of sawtooth-shaped Ca^{2+} signals in the flagellum that were accompanied by brief spikelike increases of the path curvature κ, intermitted by longer periods of low κ values (Fig. 1 A). A characteristic feature was that κ peaked, whereas F_r was still rising, and steeply fell below resting values, whereas F_r was slowly declining (Fig. 1 A); thus, $[Ca^{2+}]_i$ stayed elevated during the intermittent periods of straight swimming (Fig. 1 B). Both observations are inconsistent with a direct control of path curvature by absolute $[Ca^{2+}]_i$. In fact, analysis of the paths from 27 cells revealed no correlation between fluorescence intensity, i.e., $[Ca^{2+}]_i$ and curvature (Fig. 1 F). However, the time derivative of the fluorescence signal (dF_r/dt) and the curvature (κ) superimposed (Fig. 1 C). The good match also manifested in a high correlation coefficient between these two measures (Fig. 1 F). Moreover, dF_r/dt, but not F_r, perfectly coincided with the turn episodes, i.e., the path segment with the highest curvature (Fig. 1 [B–E] and Video 1). Because after stimulation the fluorescence from the flagellum makes the largest contribution to the Ca^{2+} signal and because the correlation is highest for the flagellum compared with the head, we conclude that $d[Ca^{2+}]/dt$ in the flagellum is responsible for the changes in κ (Figs. S4 and S5).

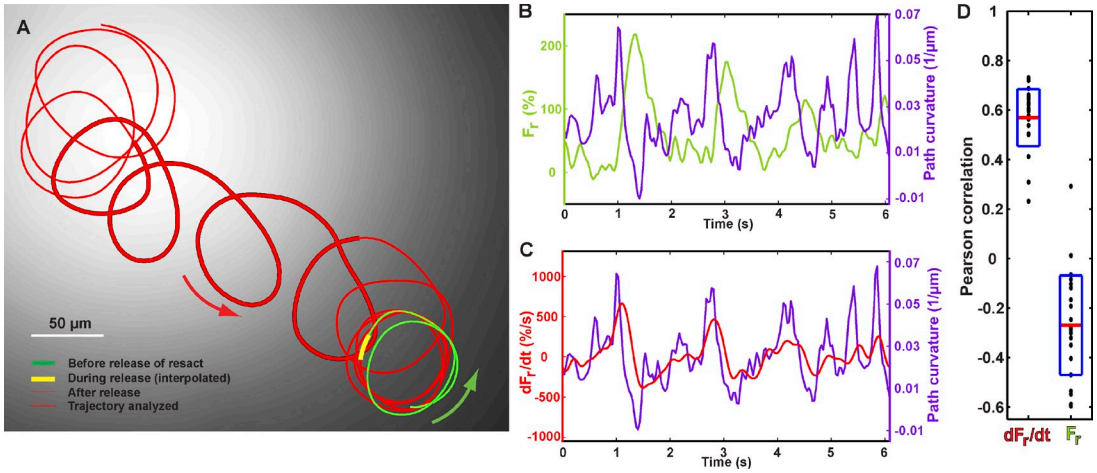

Figure 2. **Trajectory of a sperm cell in a radial gradient of resact is determined by the time derivative of $[Ca^{2+}]_i$.** (A) Swimming path of a sperm cell in a radial gradient of resact. The UV profile used for uncaging resact is indicated by shades of gray. The cell swims on circles drifting up the gradient while $[Ca^{2+}]_i$ oscillates. Arrows indicate the swimming direction. (B) Changes in F_r and path curvature κ oscillate with identical frequency, but the oscillations do not superimpose. (C) Changes in dF_r/dt and path curvature κ superimpose and are strongly correlated. (D) Pearson correlation between path curvature and dF_r/dt or F_r. Individual data points are displayed as black circles (n = 27), mean correlation is in red, and SD is in blue (box length is twice the SD).

The time course κ(t) after stimulation can be described by the linear relationship

$$\kappa(t) = \kappa_1 + \beta \frac{dF_r}{dt}, \quad (1)$$

where β is a proportionality factor, κ_1 is a parameter that characterizes the basal curvature, and $F_r = \Delta F/F_0$ is the normalized relative change in fluorescence. Fit parameters were β = 0.04 ± 0.03 s/mm and κ_1 = 12 ± 8 mm^{-1} (mean ± SD; n = 27). The goodness of the fit to Eq. 1 is given by the coefficient of determination, which is the square of the Pearson correlation coefficient R (Figs. 1 F and 2 D).

On photolysis, the cGMP increase occurs almost instantaneously and triggers intrinsic Ca^{2+} oscillations (Böhmer et al., 2005). For swimming in a gradient of resact, however, the cGMP increase is slower owing to the synthesis by the guanylyl cyclase, and Ca^{2+} oscillations are entrained to the periodic stimulation of sperm with the chemoattractant (Böhmer et al., 2005). Therefore, we tested whether the relation between dF_r/dt and κ also holds true during chemotactic navigation. We recorded Ca^{2+} signals of sperm swimming in a chemical gradient. The gradient was produced by the release of resact from caged resact using a radial (Gaussian) profile of UV light (Böhmer et al., 2005; Friedrich and Jülicher, 2007). In the resact gradient, sperm moved along drifting circles toward the top of the concentration profile (Fig. 2 A). Again, the curvature correlated with dF_r/dt and not with F_r (Fig. 2, B–D). In some cases, the peaks of $d[Ca^{2+}]_i/dt$ and κ do not perfectly align (Fig. 1 C). A shift might result from data acquisition and processing involving finite frame rates (30 Hz) and spatiotemporal smoothing that slightly limits temporal resolution. We conclude that the relation between $d[Ca^{2+}]_i/dt$ and κ is preserved, regardless of whether Ca^{2+} oscillations are evoked by a step increase of cGMP or by navigation in a gradient of chemoattractant.

Waveform of Ca^{2+} signals determines the swimming path

The waveform and frequency of Ca^{2+} signals evoked by cGMP or resact greatly vary between cells depending on the stimulus strength or steepness of the gradient. We examined which features of the Ca^{2+} waveform shape the swimming path. Photorelease of cGMP evoked an initial increase of $[Ca^{2+}]_i$ followed by oscillations of smaller amplitude that are superimposed on the elevated Ca^{2+} level (top graphs in Fig. 3, A–C). Quite generally, steep and long rising phases of $[Ca^{2+}]_i$ produced sharp turns, whereas the characteristics of the Ca^{2+} decline determined the duration and curvature of the run periods (bottom illustrations in Fig. 3, A–C). Despite the large variation of Ca^{2+} waveforms, path curvature and dF_r/dt always superimposed (middle graphs in Fig. 3, A–C).

To gain insight into how exactly the Ca^{2+} waveform shapes the path, we numerically reconstructed the swimming path generated by model Ca^{2+} signals using Eq. 1. The slope of the Ca^{2+} rise determines the sharpness of turns and, thereby, the angle between sperm orientation before and after a turn (Fig. 4 A). In addition, the orientation angle is controlled by the duration of the rising phase (Fig. 4 B).

The slope of the Ca^{2+} decline determines the curvilinearity of the path during the run period (Fig. 4 C). A fast Ca^{2+} decline can even give rise to negative values of the curvature (i.e., the path temporarily curves in clockwise rather than counterclockwise direction; Fig. 4 C, right). In fact, this prediction from the simulation is borne out by experiment. We took advantage of the observation that a second cGMP increase delivered at the peak of a Ca^{2+} signal produced a large and rapid Ca^{2+} drop, probably owing to the closure of Ca_v channels and enhanced Na^+/Ca^{2+} exchange activity (Fig. 5 A; Nishigaki et al., 2004; Kashikar, 2009). We recorded the path before and after the second stimulus. During the rapid Ca^{2+} drop, whereas F_r was still elevated, dF_r/dt was minimal, and the curvature adopted negative values (Fig. 5, A–C). As a

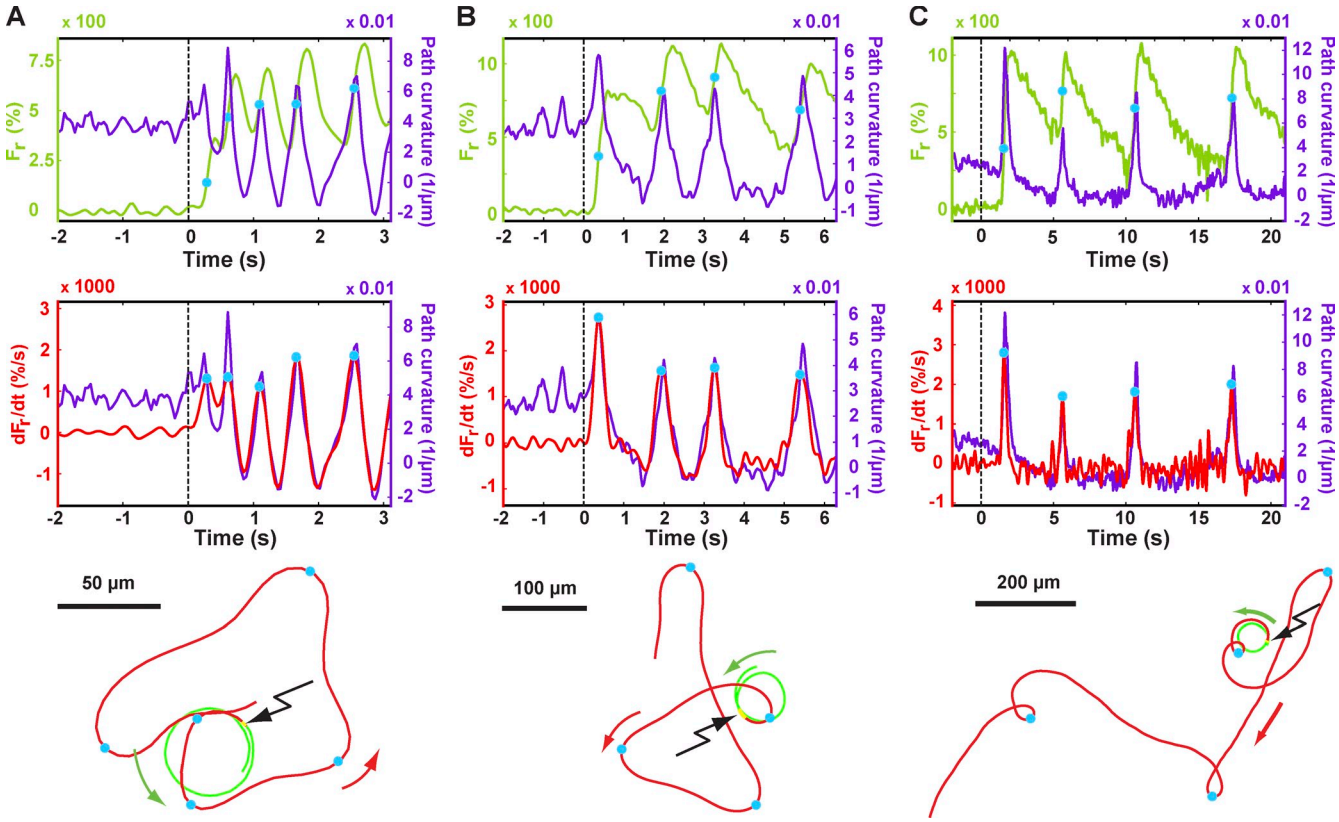

Figure 3. **Waveform of Ca^{2+} signals determines path shape.** (A–C, top graphs) Ca^{2+} signals and changes in path curvature κ evoked by release of cGMP at t = 0 (dashed lines) in three cells. Cyan dots on the Ca^{2+} signals correspond to local maxima of dF_r/dt. (middle graphs) dF_r/dt and curvature κ superimpose on each other. (bottom illustrations) Swimming paths of the same cells before (green) and after (red) release of cGMP (black arrows and yellow bars). Green and red arrows indicate the swimming direction of the cell before and after release of resact, respectively. From left A to right C, cells vary from fast and symmetric Ca^{2+} oscillations to slower and skewed oscillations. Correspondingly, path curvature varies from fast oscillations (on a high $[Ca^{2+}]_i$) to slow and asymmetric oscillations with brief episodes of steep peaks (turns) and long episodes of low curvature (runs). Swimming paths for the respective cells vary from short turn and run episodes with almost symmetrical but opposite curving (A) to sharp turns and long runs (C). Cyan dots indicate local maxima of dF_r/dt.

consequence, the swimming path curved for a short period in the clockwise direction before it returned to the counterclockwise mode (Fig. 5, D–F).

Periodic Ca^{2+} signals with various shares of positive and negatives slopes gave rise to a great variety of swimming paths ranging from slow drifting circles to saltatoric paths characterized by narrow turns and wide arcs of run periods (Fig. 4 D). Finally, using Eq. 1 and considering the swimming speed of the cell, the overall path of sperm swimming in a chemoattractant gradient was also predicted with reasonable precision from the experimentally determined Ca^{2+} signal (Fig. 6).

Pharmacological interference with chemotactic signaling does not alter the relation between $d[Ca^{2+}]_i/dt$ and κ

Next, we pharmacologically altered the Ca^{2+} waveform to test whether Ca^{2+} kinetics affects chemotactic efficacy. Niflumic acid alters Ca^{2+} oscillations in sperm either by inhibition of Ca^{2+}-activated Cl^- channels (Wood et al., 2003, 2007) or by targeting other signaling components such as hyperpolarization-activated cyclic nucleotide-gated channels (Gauss et al., 1998; Cheng and Sanguinetti, 2009). Whatever the underlying mechanism might be, Niflumic acid offers a means to study how the Ca^{2+} waveform affects the swimming path and, thereby, chemotaxis efficacy. Niflumic acid distorted the cGMP-evoked Ca^{2+} signals in a characteristic way (Fig. 7): the initial increase of $[Ca^{2+}]_i$ was followed by Ca^{2+} oscillations that appeared as small ripples on an elevated Ca^{2+} level (Fig. 7 A). Accordingly, the curvature pattern consisted of closely spaced spikes and was lacking longer intermittent periods of low κ values. Despite these profound changes in Ca^{2+} waveform, the relation between dF_r/dt and κ remained unaltered, and both quantities superimposed (Fig. 7 B). The altered Ca^{2+} dynamics entailed characteristic changes in the swimming path. Control sperm usually make sharp turns and wide arcs of running. With Niflumic acid, turns and runs were both shorter. Furthermore, the curvature changed sign, and the runs initially curved in clockwise rather than counterclockwise direction, producing a trefoil-like pattern of the path (Fig. 7 C).

How do the changes in swimming path affect the ability of sperm to accumulate in a chemical gradient? We followed the redistribution of sperm in a resact gradient produced by UV irradiation of caged resact using a Gaussian intensity profile. In the presence of Niflumic acid, the ability of sperm to accumulate was impaired although not completely abolished (Fig. 7 D). Chemotactic behavior requires a characteristic latency between

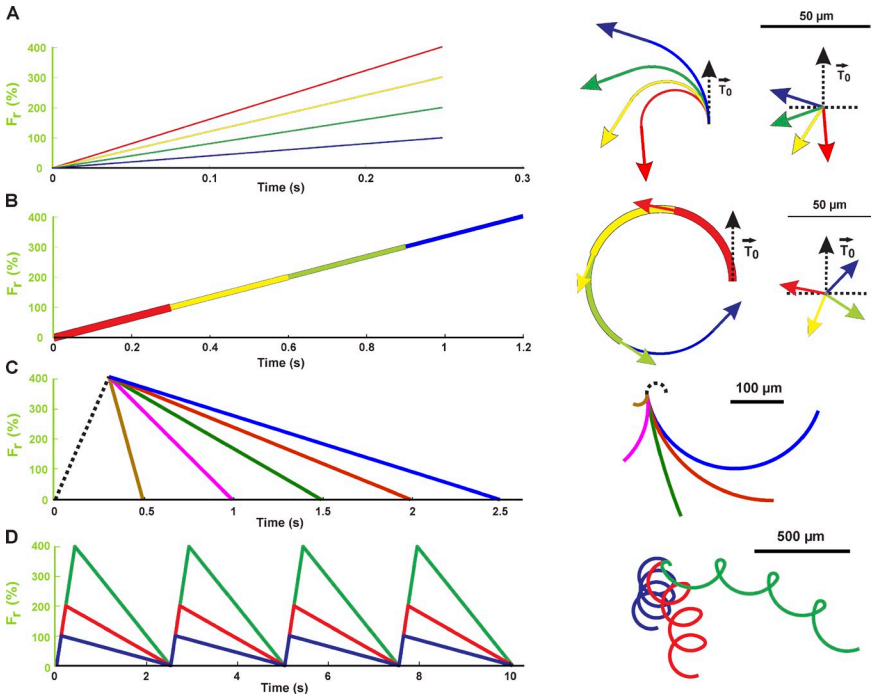

Figure 4. **Numerical reconstruction of swimming paths.** Model Ca^{2+} signals and corresponding reconstructed paths using the fit parameters κ_1 and β of Eq. 1. The swimming speed was considered constant for simplicity (v = 200 µm/s). (A) The slope of the rising phase (Ca^{2+} influx) determines the sharpness of the chemotactic turn and the orientation of the cell after the turn. (B) The length of the rising phase determines the duration of the turn and, therefore, codetermines the orientation of the cell before the run. (C) The slope of the Ca^{2+} decline determines the length, the straightness, and sign of the curvature during the run period, depending on the parameters κ_1 and β. (D) The kinetics of the rising and declining phases and the amplitude of the Ca^{2+} signal determine the drifting speed and direction of circles.

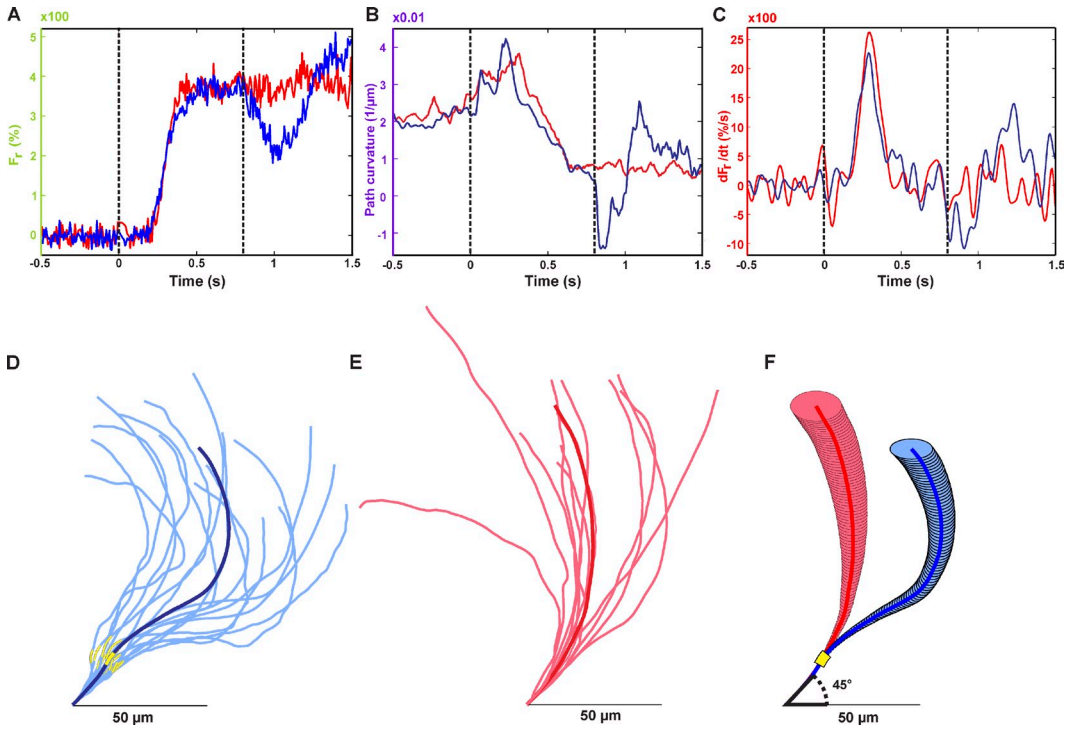

Figure 5. **Rapid Ca^{2+} decay reverses sign of path curvature.** (A) Mean Ca^{2+} signal elicited by release of caged cGMP (n = 7) by one (red) or two (blue) identical flashes 800 ms apart. (B) Time course of the mean path curvature for cells stimulated with a single flash (red, n = 11) or two flashes (blue, n = 16). (C) Mean dF_r/dt calculated from data in A for one (red) or two (blue) identical flashes. (A–C) The UV flashes are indicated by black dashed lines. (D) Superposition of single-cell trajectories (light blue, n = 17) and mean trajectory (dark blue) around the position where the second stimulus was delivered (yellow boxes). (E) Superposition of single-cell trajectories (light red, n = 11) and mean trajectory (dark red) around the same time point position as in D for those cells receiving only one stimulus. (F) Comparison of mean swimming paths for cells stimulated with a single flash (red, n = 11) or two flashes (blue, n = 17). The error at each point is represented by an ellipse with minor and major axes showing the SEM in the direction of the abscissa and the ordinate.

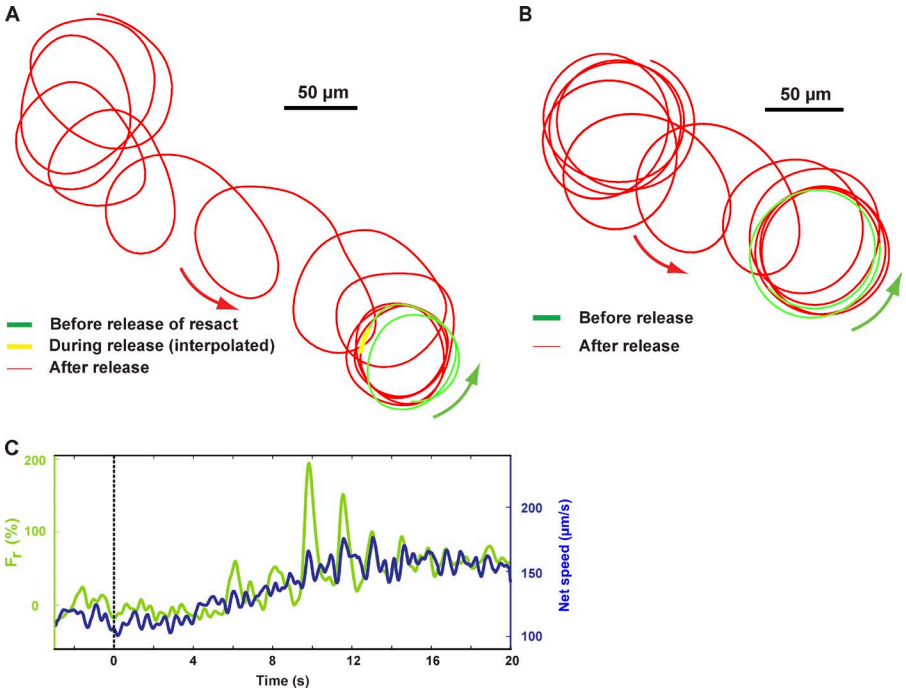

Figure 6. **Reconstruction of sperm swimming paths in a chemical gradient.** (A) Trajectory of the cell shown in Fig. 2 before and after the release of resact. (B) Numerical reconstruction of the swimming path using the time derivative dF_r/dt and the speed. The reconstructed path reproduces many of the essential features of the original path. (C) Experimental Ca^{2+} signal and speed of the sperm cell used for the reconstruction. The release of resact from the caged derivative occurs at t = 0 (dashed line).

the stimulus and the steering response (Friedrich and Jülicher, 2007). We presume that Niflumic acid detuned this time delay and, thereby, impaired chemotactic accumulation.

The chemical differentiator model

Despite the simple relationship between $d[Ca^{2+}]_i/dt$ and path curvature, it is not apparent how cells implement such a differentiator using a reaction network to control flagellar bending waves. In flagella and cilia, the shape and frequency of the beat are modulated by several Ca^{2+}-binding proteins (B), notably CaM. These proteins control molecular components of the axoneme, in particular motor proteins (DiPetrillo and Smith, 2009; King, 2010). Here, we propose a simple biochemical mechanism that could generate a cellular differentiator. The second-order kinetics for Ca^{2+} binding to a protein B reads as follows:

$$Ca^{2+} + B \underset{k_{off}}{\overset{k_{on}}{\leftrightarrow}} CaB.$$

In the terminology of signal processing, the concentration [CaB] of Ca^{2+} complexes serves as a low-pass filter that faithfully tracks relatively slow variations of the input $[Ca^{2+}]$ but effectively filters any fast changes. The second-order reaction can be linearized using two simplifying assumptions. First, in the limit where $k_{on}[Ca^{2+}]$ is much less than k_{off}, [B] is approximately constant, and the kinetics of the reaction becomes pseudo–first order with a characteristic time constant of low-pass filtering $\tau_1 = 1/k_{off}$. Second, in the limit of small variations of the total Ca^{2+} concentration around its steady-state value, the characteristic time constant $\tau_2 = 1/(k_{on}[Ca^{2+}] + k_{off} + k_{on}[B])$.

Our simple model consists of two distinct proteins, B_1 and B_2, coupled to a motor protein. We assume that binding of Ca^{2+} to B_1 and B_2 enhances and diminishes flagellar asymmetry, respectively, for example by enhancing either principal or reverse flagellar bending on opposite microtubule doublets. For sake of simplicity, we assume the following direct relationship between the concentration difference $[CaB_1] - [CaB_2]$ and flagellar asymmetry C:

$$C = \alpha \times \left(\left[CaB_1 \right] - \left[CaB_2 \right] \right). \quad (2)$$

The difference of occupancy of B_1 and B_2 by Ca^{2+} can act as a chemical differentiator, provided the kinetics of binding of $CaB_{1,2}$ to the motor protein is not identical, B_1 and B_2 are of similar concentration, and the K_d values are approximately equal. Of note, an equivalent mechanism can be established with a single Ca^{2+}-binding protein hosting two different Ca^{2+}-binding sites.

To study the performance of the chemical differentiator model, we chose the following set of parameters: the rate constants and concentrations were derived from the Ca^{2+}-binding protein light chain 4 (LC4). LC4 forms part of the outer dynein arm of *Chlamydomonas reinhardtii*. This protein complex is required for changes in flagellar symmetry associated with the photophobic response. LC4 possesses two EF-hand motifs and binds Ca^{2+} with a dissociation constant $K_d = 3 \times 10^{-5}$ M. LC4 forms a complex with the dynein heavy chain–γ and undergoes Ca^{2+}-dependent conformational changes (Sakato et al., 2007). Assuming a 1:1 stoichiometry between LC4 and outer dynein arm (24-nm axial periodicity), a flagellar length of 50 µm, and a flagellar volume of 1.6 femtoliters, we obtain $[LC4]_{total} = 20$ µM. We assume $[B_1] = [B_2] = [LC4]_{total}$ and a maximal free $[Ca^{2+}]$ of 500 nM (Cook et al., 1994). The reaction rates used were $k^1_{on} = 5 \times 10^6\ M^{-1}s^{-1}$, $k^1_{off} = 150\ s^{-1}$, $k^2_{on} = k^1_{on}/2$, and $k^2_{off} = k^1_{off}/2$, compatible with the K_d value reported for LC4. We studied the input–output relation of the chemical differentiator by using sinusoidal $[Ca^{2+}]$ test stimuli with varying frequency f as follows:

$$\left[Ca^{2+} \right] = A_0 + A_1 \cos\left(2\pi f \times t \right).$$

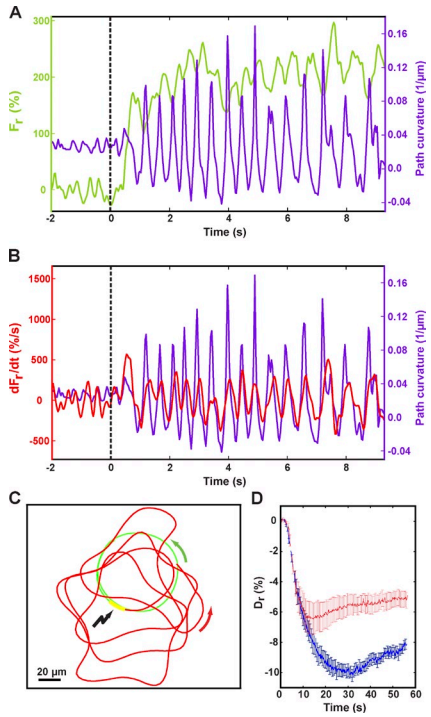

Figure 7. **Interfering with the signaling pathway.** (A) Changes in $[Ca^{2+}]_i$ and path curvature evoked by release of cGMP at t = 0 (dashed line) in the presence of 10 μM Niflumic acid. The cell displays small, rapid Ca^{2+} oscillations that entail similarly fast curvature oscillations (Pearson correlation, −0.17; mean Pearson correlation, −0.01 ± 0.28; *n* = 6). (B) Path curvature and dF_r/dt superimpose (Pearson correlation, 0.50; mean Pearson correlation, 0.48 ± 0.13; *n* = 6). (C) Swimming path of a sperm cell before (green) and after (red) cGMP release by a UV flash (black arrow and yellow bar) in the presence of 10 μM Niflumic acid. (D) Sperm accumulation in a Gaussian gradient of chemoattractant with and without Niflumic acid. Relative changes in the standard distance D_r of sperm around the center of the flash after release of resact (t = 0) without (blue) or with (red) 10 μM Niflumic acid are shown. Error bars denote SEM (12 experiments).

We find that the output signals also display sinusoidal waveforms that can be described by

$$C = \alpha \times \left(\left[CaB_1 \right] - \left[CaB_2 \right] \right) = \rho A_1 \cos\left(2\pi f \times t + \phi \right),$$

with amplitude gain ρ and phase shift ϕ depending on the input frequency *f* (Fig. 8, A and B).

Strict mathematical differentiation of the test stimuli leads to the following expression:

$$\frac{d\left[Ca^{2+} \right]}{dt} = -2\pi f A_1 \sin(2\pi f \times t) = 2\pi f A_1 \cos\left(2\pi f \times t + \frac{\pi}{2} \right).$$

Thus, differentiation requires both an output signal with a phase shift ϕ = π/2 radians or 90° and a gain that increases linearly with the input frequency. Indeed, we find that the chemical differentiator model fulfils these two requirements within the differentiation band (*f* ≤ 6 Hz; Fig. 8, A and B).

An inherent property of a strict mathematical differentiator is that the output gain approaches zero for slow input frequencies. As a consequence, at steady state, the differentiator is insensitive to the basal input. Within the differentiation band, the chemical differentiator indeed displays this property. Therefore, the chemical differentiator exhibits perfect adaptation: the steady-state output *C* is zero if the input $[Ca^{2+}]$ does not change with time. In other words, the output returns to baseline levels even in the presence of an elevated steady input level.

On the contrary, for high input frequencies (*f* > 6 Hz), the chemical differentiator deviates from the strict mathematical equivalent. This unexpected property results in a more robust mechanism because input signals with high frequencies (usually associated with stochastic noise) are filtered out. Of note, the frequency of Ca^{2+} oscillations in sperm is typically ∼1 Hz. Indeed, when using prototypical test Ca^{2+} signals, the output *C* follows the time derivative $d[Ca^{2+}]_i/dt$ of the Ca^{2+} signal (Fig. 8, C and D).

In terms of systems biology, our model represents an incoherent biparallel motif that also behaves like a band-pass filter (Milo et al., 2002). However, it lacks robustness with respect to parameter variations. Such robustness could require feedback mechanisms not considered here (Barkai and Leibler, 1997). In particular, direct mechanical feedback arising from the flagellar beat could provide such robustness (Howard, 2009). Our system

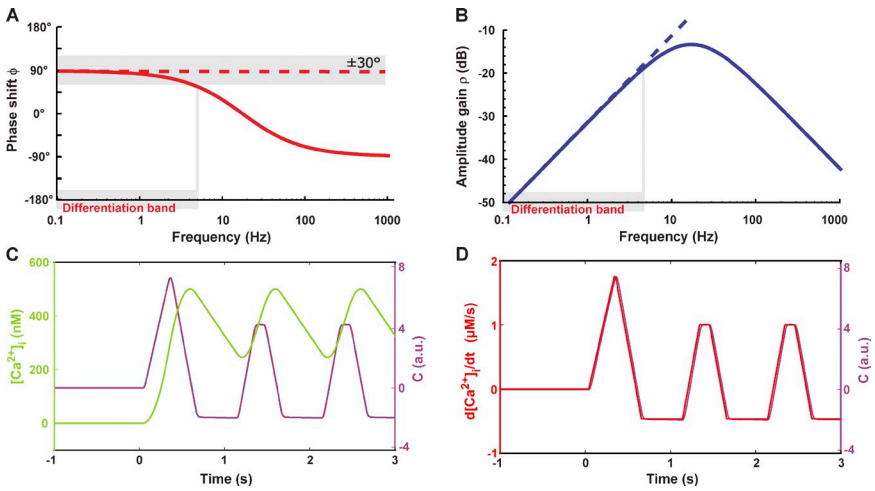

Figure 8. **Chemical differentiator model.** (A) Input–output relation of the chemical differentiator. Phase shift between input and output signals is shown. Within the differentiator band, the phase shift ϕ approximately equals 90°, with a tolerance of 30°. (B) Amplitude gain as function of the input frequency. For input frequencies 0 < f < 6 Hz (the differentiation band is in gray), the amplitude gain ρ increases linearly. (C) Model Ca^{2+} signal used as input for the chemical differentiator (green) and the output parameter *C* (purple) resulting from the model. (D) Time derivative of the input Ca^{2+} signal and the output *C* perfectly superimposes. a.u., arbitrary unit.

is intended to illustrate a simple mechanism of chemical differentiation by cellular messengers that produce opposite actions on different time scales in response to an input signal.

Discussion

In a general model of sperm chemotaxis, a signaling pathway translates a periodic stimulus into a periodic modulation of the path curvature (Friedrich and Jülicher, 2007). Here, we identified the signal transfer function between the input (Ca^{2+} signal) and the output (path curvature). Although Ca^{2+} spikes trigger the steering response, previous studies on sperm of marine invertebrates noted that the path curvature is not directly correlated with $[Ca^{2+}]_i$ and that sperm swim on straighter paths at elevated $[Ca^{2+}]_i$ (Böhmer et al., 2005; Wood et al., 2007; Shiba et al., 2008; Guerrero et al., 2010a), an observation at odds with studies on demembranated sperm (Brokaw, 1979; Lindemann and Goltz, 1988; Lindemann et al., 1991). Moreover, it was noted that κ peaked long before $[Ca^{2+}]_i$ has risen maximally (see Fig. 3 B from Guerrero et al., 2010a). Our findings provide an explanation for these observations: the curvature κ is highly correlated with $d[Ca^{2+}]_i/dt$ rather than $[Ca^{2+}]_i$, and, consequently, $[Ca^{2+}]_i$ is still high when κ is low. By inference, our data suggest that the flagellar asymmetry is controlled by $d[Ca^{2+}]_i/dt$ as well. Moreover, numerical simulations using this signal transfer function reproduce the richness of swimming modes—from looping paths to smoothly drifting circles—observed for sperm of many marine invertebrates (Miller, 1985).

How general is this mechanism of using $d[Ca^{2+}]_i/dt$ to control the swimming path of sperm? We analyzed the changes in $[Ca^{2+}]_i$ and swimming path for several datasets of two other sea urchin species and a single dataset of *Ciona intestinalis*. For all three species, we obtained similar results, suggesting that this mechanism is not restricted to *A. punctulata* sperm (Figs. S2 and S3). It will be interesting to study this relationship also in mammalian sperm or, quite general, in motile cilia whose beat also depends on $[Ca^{2+}]_i$.

However, regulation of κ might be more complex. For example, before stimulation, sperm swim with a basal curvature (κ_0) larger than after stimulation (κ_1). Moreover, the mean curvature after stimulation stays low for some time and then slowly returns to resting values within ≤60 s (Böhmer et al., 2005). Accordingly, when sperm have returned to swimming again in regular circles, their diameter is larger (i.e., the κ_1 value is lower; Kaupp et al., 2003; Böhmer et al., 2005; Guerrero et al., 2010a). When $[Ca^{2+}]_i$ eventually returns to baseline level, the circles constrict, and the curvature returns to the basic value κ_0 (Kaupp et al., 2003; Böhmer et al., 2005). Thus, in intact sperm, the relationship between flagellar asymmetry and steady-state $[Ca^{2+}]_i$ is inverse to that observed for demembranated sperm. Probably, the modulation of flagellar bending by $[Ca^{2+}]_i$ is altered in demembranated sperm and might not mirror the control in intact motile sperm. In conclusion, $[Ca^{2+}]_i$ possibly controls the flagellar beat on two different time regimes: on a rapid time scale, the curvature follows on the heels of $d[Ca^{2+}]_i/dt$, whereas at quasi–steady state, κ is inversely related to $[Ca^{2+}]_i$ (i.e., low κ corresponds to higher $[Ca^{2+}]_i$). On a final note, the ciliary and flagellar beat is also affected by cAMP and pH (Salathe, 2007). It needs to be addressed by future studies whether cAMP and pH are involved in the slow modulation of κ.

Our studies have been restricted to sperm swimming at the glass–water interface in shallow chambers. When swimming in a plane (2D), the path curvature is controlled by $d[Ca^{2+}]_i/dt$. In 3D, however, sperm swim on helical paths (Crenshaw, 1993; Corkidi et al., 2008). Chemotaxis in 2D only requires modulation of the flagellar beat in a plane, yet, for freely swimming sperm, more complex 3D waveforms of the beat might be required. Notwithstanding, the reorientation of the axis of the path helix toward the chemoattractant gradient might also be governed by $d[Ca^{2+}]_i/dt$ rather than $[Ca^{2+}]_i$ itself.

For most cellular systems, the response to a continuous stimulus is transient, a property termed adaptation. In sperm, nothing was known about adaptation along the cellular signaling pathway. The dependence of curvature on $d[Ca^{2+}]_i/dt$ constitutes a novel chemomechanical mechanism of perfect adaptation. The mechanical transducer only responds to changes in $[Ca^{2+}]_i$ (i.e., at steady state, the output is constant). Such an adaptive system enables sperm to maintain their responsiveness at elevated levels of both chemoattractant and $[Ca^{2+}]_i$ during their sojourn to the egg.

The mechanism how sperm compute a time derivative of $[Ca^{2+}]_i$ and how this time derivative controls the flagellar beat could be based on two Ca^{2+}-binding reactions with different time constants and opposite action on flagellar bending. In the axoneme of *Chlamydomonas* flagella, ∼27 proteins have been identified that carry an EF-hand, a common structural motif for Ca^{2+}-binding proteins (Pazour et al., 2005). CaM, a key Ca^{2+} sensor in cilia, is associated with the radial spoke stalk and the central pair, and several CaM-binding proteins have been identified (DiPetrillo and Smith, 2009, 2010; King, 2010). Moreover, Ca^{2+} binds more rapidly to CaM than to other Ca^{2+}-binding proteins (Faas et al., 2011). Furthermore, two Ca^{2+} ions cooperatively bind to both the N- and C-lobe of CaM. The binding kinetics and affinity of Ca^{2+} to the two lobes are orders-of-magnitude different (Faas et al., 2011). These features provide a structural basis for the chemical differentiator model. Finally, the N- and C-lobe of CaM might sense different Ca^{2+} pools (i.e., global vs. local Ca^{2+} in nanodomains), as suggested for Ca_v channels (Tadross et al., 2008). Our minimalist model illustrates a general concept by which a cell could compute the time derivative of an input signal.

The control of the flagellar beat by Ca^{2+} is not restricted to sperm. The intrinsic beat of most if not all motile cilia is modulated by $[Ca^{2+}]_i$ (Salathe, 2007). Motile cilia serve diverse functions. They transport liquid and, thereby, generate gradients of morphogens during embryonic development (Okada et al., 2005), clear mucus in airway epithelium (Marshall and Nonaka, 2006), and control the phototactic or mechanosensitive steering response of *Chlamydomonas* (Witman, 1993), *Volvox* (Drescher et al., 2010), *Paramecium* (Naito and Kaneko, 1972), and zooplankton (Jékely et al., 2008). Because the motile cytoskeletal element of cilia, the axoneme, is highly conserved, it will be interesting to know whether cilia in general use a similar signal transfer function to modulate the beat pattern.

Materials and methods

Sample preparation

Dry sea urchin sperm were collected by injection of 0.5 M KCl into the body cavity or by stimulating the animal electrically with electrodes at a potential of 25 V peak to peak; the spawned sperm were aspirated using a Pasteur pipette and stored on ice. All collected samples were used within 4 d. Sperm were activated by dilution in artificial sea water (ASW), which contained 9 mM KCl, 423 mM NaCl, 9.27 mM $CaCl_2$, 22.94 mM $MgCl_2$, 25.5 mM $MgSO_4$, 0.1 mM EDTA, and 10 mM Hepes, adjusted to pH 7.8, with NaOH. For loading, dry sperm were diluted 1:6 (volume/volume) in ASW containing 30 µM Fluo-4 acetoxymethyl ester (AM; Invitrogen) and 0.5% Pluronic F127 (Sigma-Aldrich). After incubation for 60 min at 20°C, the sample was diluted 10^4 fold with ASW supplemented with 0.5% Pluronic F127 and kept in the dark at 18°C. For experiments carried out with *Lytechinus pictus* or *Strongylocentrotus purpuratus*, 1% BSA was added to the sperm suspension to reduce interaction of sperm with the wall of the recording chamber. For photolysis experiments with cGMP, [6,7-bis(ethoxycarbonylmethoxy)-coumarin-4-yl]methyl-cGMP (caged BECMCM-cGMP; Kaupp et al., 2003) was used. The compound was synthesized by V. Hagen (Leibniz-Institut für Molekulare Pharmakologie, Berlin, Germany). Caged cGMP was present during loading at 20 µM for *A. punctulata* or 100 µM for *L. pictus* and *S. purpuratus* sperm. The same concentration of caged cGMP was kept during the final dilution of sperm to prevent leaking of caged cGMP from the cell. For experiments with gradients of resact, 1 µM 8-DMNB–caged resact was used. Niflumic acid (Sigma-Aldrich) was added to dilute sperm (10 µM) 2 min before measurements. To define the regimen of linearity between free Ca^{2+} concentration ($[Ca^{2+}]$) and Fluo-4 intensity, experiments using ionophore A23187 were performed. After Fluo-4 loading, cells were suspended in ASW containing 10 µM ionophore and a given free $[Ca^{2+}]$ that was adjusted by EGTA and calculated using webmaxc (Patton et al., 2004). Fluorescence was measured after 30 min of incubation.

Optical setup

The swimming behavior of sperm was studied in a shallow observation chamber (depth of 100 µm). Sperm swim in a plane close to the glass–water interface. The restriction to 2D motion facilitated both recording and analysis of swimming paths. Motility was recorded with an inverted microscope (IX71; Olympus) equipped with a 20× magnification objective (0.75 NA; UPLSAPO; Olympus). Photolysis of caged compounds was achieved using a 100-W mercury lamp (U-RFL-T; Olympus). The irradiation time (30 ms) was controlled by a mechanical shutter (Uniblitz VS25; Vincent Associates), and the intensity of the UV flash was adjusted using a set of neutral-density filters (Qioptiq Photonics). The 488-nm line from an argon/krypton laser (Innova 70C; Coherent, Inc.) was used for excitation of Fluo-4. To produce sharp images of swimming sperm, laser-stroboscopic illumination (2-ms pulse) was generated using an acoustooptical tunable filter (AA Opto-Electronic Company). The fluorescence was filtered by a 500-nm long-pass filter (Omega Optical, Inc.). Images were collected at 30 frames per second using a back-illuminated electron-multiplying charge-coupled device camera (DU-897D; Andor Technology). To reconstruct a cell's trajectory, a motorized stage (SCAN IM; Märzhäuser Wetzlar GmbH & Co.) was used, and the position of the stage at each frame was recorded. The setup was synchronized using an acquisition program written in LabVIEW and data acquisition hardware PCI-6040E (National Instruments).

Quantitative motility analysis

We used custom-made postacquisition programs written in MATLAB (MathWorks) to track swimming sperm and to measure time-resolved changes in fluorescence. The relative changes in fluorescence F_r were computed using the formula $F_r(t) = 100 \cdot [F(t) - F(0)]/F(0)$, where $F(t)$ is the total fluorescence of the cell at time t. Our analysis has to account for the complex fine structure of sperm swimming paths: for a swimming sperm cell, the sperm head wiggles around an averaged path with the same frequency as the flagellar beat as a result of balancing forces generated by the flagellar beat (Gray, 1955; Friedrich et al., 2010).

We used a second-order Savitzky–Golay filter to extract the averaged path from tracking of the sperm head. Sperm swim preferentially in an anticlockwise direction on the upper surface of the recording chamber (Gray, 1955). This preferred direction is reversed on the opposite surface. To compare cells from both glass/water interfaces, we flipped planar swimming paths to assure anticlockwise curvature before stimulation. Signed curvature was then calculated from the averaged path using the following formula:

$$\kappa = (\dot{x}\ddot{y} - \ddot{x}\dot{y}) / v^3 .$$

The smoothed time derivative of the fluorescence signal was calculated as follows. First, the fluorescence signal was filtered with a Gaussian kernel with an SD of 80 ms. Then, the symmetric difference quotients of F_r at each point were calculated. We used the fluorescence signal from the entire sperm cell because splitting of the signal into contributions from head and flagellum introduces an additional error, which lowers the signal-to-noise ratio and interferes with computing the derivative. However, separate analysis of fluorescence derived from head and flagellum does not alter the result (Fig. S5). To analyze the fluorescent signals from flagellum and head, we automatically generated masks to spatially filter these regions. The algorithm used to generate the masks takes advantage of the fact that the intensity/pixel from the image of the head is higher than that from the flagellum. A circular region of interest with a diameter of 12 µm (~100 μm^2) was automatically selected around the center of the head. In this region of interest, an intensity threshold was iteratively approached such that bright clusters of pixels inside the region of interest were found with a total area of at least 35 μm^2. From these clusters, small clusters derived from the noise were removed by an erode/dilate operation. The biggest cluster was selected as the head. To ensure a constant area of the head image of 35 μm^2 for each frame, a corona of pixels around the head was included. The total head fluorescence signal was calculated by integrating all the pixels within the constant head surface. In principle, an area of ~15–20 μm^2 would suffice to capture the head; however, we increased this area to 35 μm^2 because the algorithm proved to be more robust to small variations in focus that increased the size of the head. Fluorescence of the flagellum was then calculated as the total cell fluorescence minus the head fluorescence. Superposition of time derivative of the Ca^{2+} signal (dF_r/dt) and path curvature (κ) in all figures was performed by fitting Eq. 1 to the experimental data after stimulation, resulting in a third time series $\kappa_{fit}(t) = \kappa_1 + \beta \times dF_r/dt$. The κ_{fit} (red) and κ (purple) in Figs. 1–3, 7, S2, S3, and S5 have identical units and, therefore, can be directly compared. The numerical values of κ_{fit} and κ can be read on the right axis (purple). Because κ_{fit} results from a linear transformation of dF_r/dt, the corresponding values in the time-derivative space can be unequivocally calculated using the inverse transformation $dF_r/dt = (\kappa_{fit} - \kappa_1)/\beta$. Thus, it is possible to map every value of κ_{fit} on the original value dF_r/dt. The corresponding axis is shown on the left (red). Therefore, the red curve simultaneously represents dF_r/dt (values can be read on the left axis) and κ_{fit} (values can be read on the right axis). This superposition method allows reading values of dF_r/dt and κ while visualizing the result of the fit using Eq. 1.

To reconstruct the swimming path from the speed and the Ca^{2+} signals, we numerically calculated and rescaled the time derivative of the fluorescence signal using the parameters κ_1 and β resulting from a least mean squares fit of Eq. 1 to the data. Finally, the path was reconstructed from the curvature κ and the displacement ($s = v \times \Delta t$) by numerical integration of the 2D Frenet–Serret equations.

The efficiency of sperm chemotaxis was determined by an accumulation assay: a sperm suspension (5×10^5 cells/ml) was imaged under the microscope using dark-field microscopy while performing chemotaxis in a Gaussian gradient. The gradient was established by photolysis of 1 µM caged resact using five consecutive UV flashes to maintain the gradient for a longer period of time (flash duration of 250 ms and time between flashes of 1 s). The flashes displayed a Gaussian intensity profile with a characteristic width of σ = 115 µm. The distribution of cells around the center of the flash was quantified using relative changes of the weighted standard distance as

$$D(t) = \frac{\sqrt{\sum_{i,j} I_{ij}(t) \times \left[\left(r_i - r_x\right)^2 + \left(r_j - r_y\right)^2 \right]}}{\sum_{i,j} I_{ij}(t)},$$

where (r_x, r_y) are the coordinates of the center of the flash, (r_i, r_j) are the coordinates of the pixels in each frame, and I_{ij} represents the intensity of the pixel (r_i, r_j). Assuming that the brightness of each pixel is proportional to the density of cells, the quantity D represents the dispersion of cells. D depends on the size of the field of view. To account for this, the sum over the indices

i and *j* is taken for pixels located at a distance ≤3σ of the center of the UV flash. Finally, the relative changes of *D* were calculated using the formula $D_r = 100\ \Delta D/D_0$.

Double-flash experiments

To calculate the mean swimming path after the second flash, individual trajectories were aligned at a time point shortly before the second flash (100 ms). Such an alignment consisted of a translation to the origin of coordinates and a rotation that made coincident the tangent of each trajectory at this time point with an angle of 45° with respect to the abscissa.

Chemical differentiator

Based on the second-order chemical equations proposed in our model, the kinetics of each binding reaction was resolved numerically by direct integration of the mass balance equations. Changes in the free concentration of $B_{1,2}$ and $CaB_{1,2}$ were calculated for every iteration using the expressions

$$\left[B_i\right]_{t+\Delta t} = \left[B_i\right]_t + \Delta t\left(k_{off}\left[CaB_i\right]_t - k_{on}\left[Ca^{2+}\right]_t\left[B_i\right]_t\right) \text{ and}$$

$$\left[CaB_i\right]_{t+\Delta t} = \left[CaB_i\right]_t + \Delta t\left(k_{on}\left[Ca^{2+}\right]_t\left[B_i\right]_t - k_{off}\left[CaB_i\right]_t\right),$$

where $[Ca^{2+}]$ is the input of the model, the integration time step Δt was 1 ns, and the initial conditions were $[B_1]_0 = [B_2]_0 = [LC4]_{total}$ and $[CaB_1]_0 = [CaB_2]_0 = 0$. Finally, the parameter *C* was calculated at each time point from its definition given in Eq. 2.

Online supplemental material

Fig. S1 presents data of Fluo-4 fluorescence versus free $[Ca^{2+}]$ for sperm treated with the Ca^{2+} ionophore A23187. The fluorescent signal scales linearly with Ca^{2+} within the regimen of $[Ca^{2+}]_i$ observed in sperm during chemotaxis. Fig. S2 shows evidence for a common mechanism of flagellar control by $d[Ca^{2+}]/dt$ in other sea urchins. Fig. S3 presents evidence for a common mechanism in ascidian sperm. Fig. S4 shows the contributions to F_r of the different parts of the cell (head and flagellum) and the correlation between F_r or dF_r/dt versus the path curvature for each part. Fig. S5 displays a comparison of F_r or dF_r/dt and path curvature for a particular sperm cell. Video 1 illustrates and recapitulates our findings; a sperm cell, loaded with the calcium indicator Fluo-4 AM and caged cGMP, is shown before and after the release of cGMP with a UV flash. Online supplemental material is available at http://www.jcb.org/cgi/content/full/jcb.201106096/DC1.

We thank H. Krause for preparing the manuscript, B. Faßbender, P. Perez-Prat, and A. Takemi for assistance with the analysis, and Drs. T. Strünker, R. Seifert, and D. Wachten for critical reading of the manuscript. We thank Drs. M. Yoshida and K. Shiba for kindly providing us with their data on ascidian sperm. The caged compounds were kindly provided by Dr. V. Hagen.

L. Alvarez and U. Benjamin Kaupp conceived the project and designed experiments. L. Alvarez, L. Dai, B.M. Friedrich, N.D. Kashikar, I. Gregor, and R. Pascal performed experiments and analyzed the data. L. Alvarez, L. Dai, and B.M. Friedrich developed the tools for analysis. L. Alvarez, L. Dai, and I. Gregor established the experimental setup. L. Alvarez, B.M. Friedrich, and U. Benjamin Kaupp developed the theoretical model. L. Alvarez, U. Benjamin Kaupp, and B.M. Friedrich wrote the manuscript. All authors revised and edited the manuscript.

Submitted: 15 June 2011
Accepted: 30 January 2012

References

Barkai, N., and S. Leibler. 1997. Robustness in simple biochemical networks. *Nature*. 387:913–917. http://dx.doi.org/10.1038/43199

Böhmer, M., Q. Van, I. Weyand, V. Hagen, M. Beyermann, M. Matsumoto, M. Hoshi, E. Hildebrand, and U.B. Kaupp. 2005. Ca^{2+} spikes in the flagellum control chemotactic behavior of sperm. *EMBO J.* 24:2741–2752. http://dx.doi.org/10.1038/sj.emboj.7600744

Bönigk, W., A. Loogen, R. Seifert, N. Kashikar, C. Klemm, E. Krause, V. Hagen, E. Kremmer, T. Strünker, and U.B. Kaupp. 2009. An atypical CNG channel activated by a single cGMP molecule controls sperm chemotaxis. *Sci. Signal.* 2:ra68. http://dx.doi.org/10.1126/scisignal.2000516

Brokaw, C.J. 1979. Calcium-induced asymmetrical beating of triton-demembranated sea urchin sperm flagella. *J. Cell Biol.* 82:401–411. http://dx.doi.org/10.1083/jcb.82.2.401

Cheng, L., and M.C. Sanguinetti. 2009. Niflumic acid alters gating of HCN2 pacemaker channels by interaction with the outer region of S4 voltage sensing domains. *Mol. Pharmacol.* 75:1210–1221. http://dx.doi.org/10.1124/mol.108.054437

Cook, S.P., C.J. Brokaw, C.H. Muller, and D.F. Babcock. 1994. Sperm chemotaxis: Egg peptides control cytosolic calcium to regulate flagellar responses. *Dev. Biol.* 165:10–19. http://dx.doi.org/10.1006/dbio.1994.1229

Corkidi, G., B. Taboada, C.D. Wood, A. Guerrero, and A. Darszon. 2008. Tracking sperm in three-dimensions. *Biochem. Biophys. Res. Commun.* 373:125–129. http://dx.doi.org/10.1016/j.bbrc.2008.05.189

Crenshaw, H.C. 1993. Orientation by helical motion—III. Microorganisms can orient to stimuli by changing the direction of their rotational velocity. *Bull. Math. Biol.* 55:231–255.

DiPetrillo, C., and E. Smith. 2009. Calcium regulation of ciliary motility analysis of axonemal calcium-binding proteins. *Methods Cell Biol.* 92:163–180. http://dx.doi.org/10.1016/S0091-679X(08)92011-2

DiPetrillo, C.G., and E.F. Smith. 2010. Pcdp1 is a central apparatus protein that binds Ca^{2+}-calmodulin and regulates ciliary motility. *J. Cell Biol.* 189:601–612. http://dx.doi.org/10.1083/jcb.200912009

Drescher, K., R.E. Goldstein, and I. Tuval. 2010. Fidelity of adaptive phototaxis. *Proc. Natl. Acad. Sci. USA*. 107:11171–11176. http://dx.doi.org/10.1073/pnas.1000901107

Faas, G.C., S. Raghavachari, J.E. Lisman, and I. Mody. 2011. Calmodulin as a direct detector of Ca^{2+} signals. *Nat. Neurosci.* 14:301–304. http://dx.doi.org/10.1038/nn.2746

Friedrich, B.M., and F. Jülicher. 2007. Chemotaxis of sperm cells. *Proc. Natl. Acad. Sci. USA*. 104:13256–13261. http://dx.doi.org/10.1073/pnas.0703530104

Friedrich, B.M., I.H. Riedel-Kruse, J. Howard, and F. Jülicher. 2010. High-precision tracking of sperm swimming fine structure provides strong test of resistive force theory. *J. Exp. Biol.* 213:1226–1234. http://dx.doi.org/10.1242/jeb.039800

Galindo, B.E., J.L. de la Vega-Beltrán, P. Labarca, V.D. Vacquier, and A. Darszon. 2007. Sp-tetraKCNG: A novel cyclic nucleotide gated $K(^+)$ channel. *Biochem. Biophys. Res. Commun.* 354:668–675. http://dx.doi.org/10.1016/j.bbrc.2007.01.035

Gauss, R., R. Seifert, and U.B. Kaupp. 1998. Molecular identification of a hyperpolarization-activated channel in sea urchin sperm. *Nature*. 393:583–587. http://dx.doi.org/10.1038/31248

Gibbons, B.H., and I.R. Gibbons. 1972. Flagellar movement and adenosine triphosphatase activity in sea urchin sperm extracted with triton X-100. *J. Cell Biol.* 54:75–97. http://dx.doi.org/10.1083/jcb.54.1.75

Goltz, J.S., T.K. Gardner, K.S. Kanous, and C.B. Lindemann. 1988. The interaction of pH and cyclic adenosine 3′,5′-monophosphate on activation of motility in Triton X-100 extracted bull sperm. *Biol. Reprod.* 39:1129–1136. http://dx.doi.org/10.1095/biolreprod39.5.1129

Gray, J. 1955. The movement of sea-urchin spermatozoa. *J. Exp. Biol.* 32:775–801.

Guerrero, A., T. Nishigaki, J. Carneiro, Yoshiro Tatsu, C.D. Wood, and A. Darszon. 2010a. Tuning sperm chemotaxis by calcium burst timing. *Dev. Biol.* 344:52–65. http://dx.doi.org/10.1016/j.ydbio.2010.04.013

Guerrero, A., C.D. Wood, T. Nishigaki, J. Carneiro, and A. Darszon. 2010b. Tuning sperm chemotaxis. *Biochem. Soc. Trans.* 38:1270–1274. http://dx.doi.org/10.1042/BST0381270

Howard, J. 2009. Mechanical signaling in networks of motor and cytoskeletal proteins. *Annu. Rev. Biophys.* 38:217–234. http://dx.doi.org/10.1146/annurev.biophys.050708.133732

Jékely, G., J. Colombelli, H. Hausen, K. Guy, E. Stelzer, F. Nédélec, and D. Arendt. 2008. Mechanism of phototaxis in marine zooplankton. *Nature*. 456:395–399. http://dx.doi.org/10.1038/nature07590

Kambara, Y., K. Shiba, M. Yoshida, C. Sato, K. Kitajima, and C. Shingyoji. 2011. Mechanism regulating Ca^{2+}-dependent mechanosensory behaviour in sea urchin spermatozoa. *Cell Struct. Funct.* 36:69–82. http://dx.doi.org/10.1247/csf.10020

Kashikar, N.D. 2009. Sensitivity regulation in sperm during chemotaxis. PhD thesis. Universität zu Köln, Cologne, Germany. 105 pp.

Kaupp, U.B., J. Solzin, E. Hildebrand, J.E. Brown, A. Helbig, V. Hagen, M. Beyermann, F. Pampaloni, and I. Weyand. 2003. The signal flow and motor response controling chemotaxis of sea urchin sperm. *Nat. Cell Biol.* 5:109–117. http://dx.doi.org/10.1038/ncb915

Kaupp, U.B., N.D. Kashikar, and I. Weyand. 2008. Mechanisms of sperm chemotaxis. *Annu. Rev. Physiol.* 70:93–117. http://dx.doi.org/10.1146/annurev.physiol.70.113006.100654

Kilic, F., N.D. Kashikar, R. Schmidt, L. Alvarez, L. Dai, I. Weyand, B. Wiesner, N. Goodwin, V. Hagen, and U.B. Kaupp. 2009. Caged progesterone:

A new tool for studying rapid nongenomic actions of progesterone. *J. Am. Chem. Soc.* 131:4027–4030. http://dx.doi.org/10.1021/ja808334f

King, S.M. 2010. Sensing the mechanical state of the axoneme and integration of Ca2+ signaling by outer arm dynein. *Cytoskeleton (Hoboken)*. 67:207–213.

Lindemann, C.B., and J.S. Goltz. 1988. Calcium regulation of flagellar curvature and swimming pattern in triton X-100—extracted rat sperm. *Cell Motil. Cytoskeleton*. 10:420–431. http://dx.doi.org/10.1002/cm.970100309

Lindemann, C.B., and K.A. Lesich. 2009. Detergent-extracted models for the study of cilia or flagella. *Methods Mol. Biol.* 586:337–353. http://dx.doi.org/10.1007/978-1-60761-376-3_19

Lindemann, C.B., T.K. Gardner, E. Westbrook, and K.S. Kanous. 1991. The calcium-induced curvature reversal of rat sperm is potentiated by cAMP and inhibited by anti-calmodulin. *Cell Motil. Cytoskeleton*. 20:316–324. http://dx.doi.org/10.1002/cm.970200407

Marshall, W.F., and S. Nonaka. 2006. Cilia: Tuning in to the cell's antenna. *Curr. Biol.* 16:R604–R614. http://dx.doi.org/10.1016/j.cub.2006.07.012

Matsumoto, M., J. Solzin, A. Helbig, V. Hagen, S.-I. Ueno, O. Kawase, Y. Maruyama, M. Ogiso, M. Godde, H. Minakata, et al. 2003. A sperm-activating peptide controls a cGMP-signaling pathway in starfish sperm. *Dev. Biol.* 260:314–324. http://dx.doi.org/10.1016/S0012-1606(03)00236-7

Miller, R.L. 1985. Sperm chemo-orientation in the metazoa. *In* Biology of Fertilization. Vol. 2: Biology of the Sperm. C.B. Metz and A. Monroy, editors. Academic Press, New York. 275–337.

Milo, R., S. Shen-Orr, S. Itzkovitz, N. Kashtan, D. Chklovskii, and U. Alon. 2002. Network motifs: Simple building blocks of complex networks. *Science*. 298:824–827. http://dx.doi.org/10.1126/science.298.5594.824

Naito, Y., and H. Kaneko. 1972. Reactivated triton-extracted models o paramecium: Modification of ciliary movement by calcium ions. *Science*. 176:523–524. http://dx.doi.org/10.1126/science.176.4034.523

Naraghi, M. 1997. T-jump study of calcium binding kinetics of calcium chelators. *Cell Calcium*. 22:255–268. http://dx.doi.org/10.1016/S0143-4160(97)90064-6

Nishigaki, T., C.D. Wood, Y. Tatsu, N. Yumoto, T. Furuta, D. Elias, K. Shiba, S.A. Baba, and A. Darszon. 2004. A sea urchin egg jelly peptide induces a cGMP-mediated decrease in sperm intracellular $Ca^{(2+)}$ before its increase. *Dev. Biol.* 272:376–388. http://dx.doi.org/10.1016/j.ydbio.2004.04.035

Okada, Y., S. Takeda, Y. Tanaka, J.C. Izpisúa Belmonte, and N. Hirokawa. 2005. Mechanism of nodal flow: A conserved symmetry breaking event in left-right axis determination. *Cell*. 121:633–644. http://dx.doi.org/10.1016/j.cell.2005.04.008

Okuno, M., and C.J. Brokaw. 1981. Effects of triton-extraction conditions on beat symmetry of sea urchin sperm flagella. *Cell Motil.* 1:363–370. http://dx.doi.org/10.1002/cm.970010307

Patton, C., S. Thompson, and D. Epel. 2004. Some precautions in using chelators to buffer metals in biological solutions. *Cell Calcium*. 35:427–431. http://dx.doi.org/10.1016/j.ceca.2003.10.006

Pazour, G.J., N. Agrin, J. Leszyk, and G.B. Witman. 2005. Proteomic analysis of a eukaryotic cilium. *J. Cell Biol.* 170:103–113. http://dx.doi.org/10.1083/jcb.200504008

Sakato, M., H. Sakakibara, and S.M. King. 2007. *Chlamydomonas* outer arm dynein alters conformation in response to Ca^{2+}. *Mol. Biol. Cell*. 18:3620–3634. http://dx.doi.org/10.1091/mbc.E06-10-0917

Salathe, M. 2007. Regulation of mammalian ciliary beating. *Annu. Rev. Physiol.* 69:401–422. http://dx.doi.org/10.1146/annurev.physiol.69.040705.141253

Shiba, K., S.A. Baba, T. Inoue, and M. Yoshida. 2008. Ca^{2+} bursts occur around a local minimal concentration of attractant and trigger sperm chemotactic response. *Proc. Natl. Acad. Sci. USA*. 105:19312–19317. http://dx.doi.org/10.1073/pnas.0808580105

Strünker, T., I. Weyand, W. Bönigk, Q. Van, A. Loogen, J.E. Brown, N. Kashikar, V. Hagen, E. Krause, and U.B. Kaupp. 2006. A K^+-selective cGMP-gated ion channel controls chemosensation of sperm. *Nat. Cell Biol.* 8:1149–1154. http://dx.doi.org/10.1038/ncb1473

Strünker, T., N. Goodwin, C. Brenker, N.D. Kashikar, I. Weyand, R. Seifert, and U.B. Kaupp. 2011. The CatSper channel mediates progesterone-induced Ca^{2+} influx in human sperm. *Nature*. 471:382–386. http://dx.doi.org/10.1038/nature09769

Tadross, M.R., I.E. Dick, and D.T. Yue. 2008. Mechanism of local and global Ca2+ sensing by calmodulin in complex with a Ca^{2+} channel. *Cell*. 133:1228–1240. http://dx.doi.org/10.1016/j.cell.2008.05.025

Witman, G.B. 1993. *Chlamydomonas* phototaxis. *Trends Cell Biol.* 3:403–408. http://dx.doi.org/10.1016/0962-8924(93)90091-E

Wood, C.D., A. Darszon, and M. Whitaker. 2003. Speract induces calcium oscillations in the sperm tail. *J. Cell Biol.* 161:89–101. http://dx.doi.org/10.1083/jcb.200212053

Wood, C.D., T. Nishigaki, T. Furuta, S.A. Baba, and A. Darszon. 2005. Real-time analysis of the role of Ca^{2+} in flagellar movement and motility in single sea urchin sperm. *J. Cell Biol.* 169:725–731. http://dx.doi.org/10.1083/jcb.200411001

Wood, C.D., T. Nishigaki, Y. Tatsu, N. Yumoto, S.A. Baba, M. Whitaker, and A. Darszon. 2007. Altering the speract-induced ion permeability changes that generate flagellar Ca^{2+} spikes regulates their kinetics and sea urchin sperm motility. *Dev. Biol.* 306:525–537. http://dx.doi.org/10.1016/j.ydbio.2007.03.036